



## 1    Electrical Resistivity Tomography surveys for the geoelectric 2    characterization of the Montaguto landslide (southern Italy)

3

4                    \**Jessica Bellanova<sup>1</sup>, Giuseppe Calamita<sup>1</sup>, Alessandro Giocoli<sup>2</sup>, Raffaele Luongo<sup>1</sup>, Angela Perrone<sup>1</sup>, Vincenzo  
5                    Lapenna<sup>1</sup>, Sabatino Piscitelli<sup>1</sup>*

6                    <sup>1</sup>*Institute of Methodologies for Environmental Analysis (IMAA-CNR), Tito Scalo (PZ), Italy.*

7                    <sup>2</sup>*Italian National Agency for New Technologies, Energy and Sustainable Economic Development (ENEA), Rotondella  
8                    (MT), Italy*

9

10

11                    \*Corresponding author

12                    Bellanova Jessica

13                    Institute of Methodologies for Environmental Analysis

14                    Italian National Research Council

15                    C.da S. Loja

16                    85050, Tito (PZ)

17                    Italy

18                    jessica.bellanova@imaa.cnr.it

19

20



21 **Abstract**

22 This paper reports the results of a geoelectrical survey carried out to investigate the Montaguto  
23 earth-flow, located in the southern Apennines (Campania Region, southern Italy). The aim of the  
24 survey was to reconstruct the geometry of the landslide body, to improve the knowledge on the  
25 geological setting and to indirectly test the effectiveness of a drainage system. Although electrical  
26 resistivity contrasts in the electrical images were not very pronounced, due to the lithological  
27 characteristic of the outcropping lithotypes, it was possible to observe the presence of both lateral  
28 and vertical discontinuities that were associated with lithological boundaries, physical variation of  
29 the same material and sliding surfaces. The geoelectrical information obtained was provided to the  
30 Italian National Civil Protection Department technicians and was considered for the planning of  
31 more appropriate actions for the stabilization and safety of the slide.

32

33 **Keywords:** Electrical Resistivity Tomography; Landslide; Earth-flow; Montaguto; southern Italy

34

35



36 **1. Introduction**

37 The Montaguto landslide, located in southern Apennines (Campania Region, southern Italy), is one  
38 of the larger and complex earth-flow in Europe (Fig. 1). It was active for almost 60 years starting  
39 from, at least, 1954. Long periods of relatively slow movement and shorter periods of relatively  
40 rapid movement periodically have followed one another in the earth-flow activity (Guerriero et al.,  
41 2013).

42

43

**Figure 1** - Location of the Montaguto earth-flow, southern Apennines (Campania Region, southern Italy). White line:  
landslide boundary. Black line: railway. Yellow line: road SS90. Blue line: Cervaro River.

44

45

46 During the mid spring season of 2006, the most extensive reported slope failure started; an  
47 estimated volume of  $6 \times 10^6 \text{ m}^3$  earth-flow was activated. Four years later, in the spring of 2010, the  
48 earth-flow reached the Cervaro River valley, obstructing and strongly damaging the strategic  
49 National Railway infrastructure, connecting the towns of Naples and Bari, and the SS90 National  
50 Road, connecting Campania and Apulia Regions (Ventura et al., 2011; Guerriero et al., 2013).

51 Considerable efforts were carried by the Italian National Civil Protection Department (DPC) to  
52 tackle the emergency. Actions like artificial drainages, removal of slide material from the toe, etc.,  
53 have been taking place since then, in order to mitigate the effects of the mass movement.  
54 Notwithstanding the resulting slowdown of the earth-flow obtained, further coordinated actions are  
55 yet ongoing to ensure safer conditions to the railway and road infrastructures. However, in order to  
56 implement a well structured and comprehensive plan of intervention actions, further relevant  
57 geological, geotechnical and geophysical details (mechanical characteristics of the material,  
58 geometry of the body, etc.) are needed.

59 This paper reports the results of two geoelectrical surveys carried out in the area, in July 2011 and  
60 October 2012. As explicitly required by the DPC, the first survey was focused on the upper portion  
61 of the landslide body, to check a drainage intervention and to obtain the preliminary geophysical  
62 information on the terrains involved in the movement. The second survey was carried out in the  
63 central part of the landslide, between about 600 and 520 m a.s.l. that, despite the drainage  
64 interventions, was characterized by a trend of continuous movement. This state of activity made it  
65 different from other sectors of the landslide body and needed a deepening of the monitoring  
66 activities (Lollino et al., 2013; Lollino et al., 2014).

67



68 **2. Geological and Geomorphological setting**

69 The area affected by the Montaguto earth-flow is located in a region known as "Daunia Apennines"  
70 in the eastern part of southern Apennines.

71 The Daunia Apennines belong to the highly deformed transition area between the frontal thrusts of  
72 the Apennine chain and the western part of the foredeep (Crostella and Vezzani, 1964; Dazzaro et  
73 al., 1988). The lithological units, present in this area, are characterized by the presence of flysch  
74 units of Miocene age, rich in clay component, intensely deformed, as a result of the tectonic history  
75 of the Apennines (Amore et al., 1998; Di Nocera et al., 2011), and prone to landsliding. Usually, the  
76 activity of landslides is characterized by seasonal remobilizations of slope movements, typically  
77 due to rainfall events.

78 In the study area crop out the Faeto Flysch (FF), belonging to the Daunia Unit (Crostella and  
79 Vezzani, 1964), the Villamaina Unit (FV) (Di Nocera and Torre, 1987; Pescatore et al., 1996),  
80 colluvial deposit (d) and alluvial sediments (a). The Faeto Flysch and the unconformable overlying  
81 Villamaina Unit crop out in the upper part and in the middle-lower sector of the landslide,  
82 respectively; the alluvial sediments are present in the Cervaro River valley (Guerriero et al., 2014)  
83 (Fig. 2).

84 The Faeto Flysch, aged from Langhian to Tortonian, is composed by basinal and shelf margin facies  
85 and consists of three lithofacies, which from the bottom upward are: a calcareous-clayey-marly  
86 succession (FFa), composed by calcarenite and clay, passing upward to calcarenite, calcirudite and  
87 white marl; a calcareous-marly succession (FFb), represented by a dense alternation of calcarenite  
88 and marl, and a clayey-marly-calcareous succession (FFc), that consist of calcarenite, white marl  
89 and green clay (Santo and Senatore, 1988). The slope affected by the study earth-flow is only  
90 characterized by the outcropping of the basal member of the Faeto Flysch (FFa) (aged Burdigalian  
91 sup. - Langhian inf.), which has, locally, a prevalently calcareous-marly (FFa1) or clayey (FFa2)  
92 composition.

93 The Villamaina Unit, Early Messinian in age, is made up of conglomerates (FVa), sandstones not  
94 very well cemented with a few clay beds (FVb) and, upward, brownish-gray sandy with silty clay  
95 beds (FVc) (Lollino et al., 2014).

96 The recent 2010 Montaguto landslide is characterized by a length of  $3.1 \times 10^3$  m, a width ranging  
97 between 45 and 420 m and an aerial extension of about  $6.6 \times 10^5$  m<sup>2</sup> (~66 ha). It was estimated a  
98 volume of displaced material of about  $4 \times 10^6$  m<sup>3</sup> and a sliding surface depth varying from about 5  
99 m, near the channel area, to 20-30 m, at the toe (Ventura et al., 2011; Giordan et al., 2013;  
100 Guerriero et al., 2013; Lollino et al., 2014). As stated by Ventura et al. (2011), the depth of the  
101 water table roughly corresponds to the thickness of sliding material with sag ponds occurring in the



102 upper and central zone. The altitude gap between the landslide head scarp, 830 m a.s.l., and the toe,  
103 420 a.s.l., is about 410 m (Giordan et al., 2013).  
104 The reported velocities of most movement, from 1954 to 2010, ranged from 1 – 2 mm/month to 2 –  
105 5 cm/day. A sharp increase was registered during the large mobilization on both 2006 and 2010,  
106 from 1 m/day to 1 m/hour, as reported by Guerriero et al. (2013), or 5 m/day, as reported by  
107 Giordan et al. (2013).  
108  
109

**Figure 2** - Geological map of the Montaguto earth-flow. Legend: colluvial deposits (d); alluvial deposits (a); Villamaina Unit (FVa: conglomerate; FVb: sandstone and clay; FVc: sand and silty clay); Faeto Flysch (FFa: calcarenite, clay and marl); line with hachures: normal fault (dashed when inferred); line with triangles: axis of fold structure. The white area indicates the active earth-flow. The pink area indicates the inactive toe of the old landslide (IT). Blue lines: profiles of the ERT carried out in July 2011. Red lines: profiles of ERT carried out in October 2012. Green dot: borehole. Blue triangle: piezometers. Coordinates in UTM 33 N are shown (modified from Guerriero et al., 2014).

110

111

### 112 **3. The Electrical Resistivity Tomography method**

113 Electrical Resistivity Tomography (ERT) technique has been largely applied for the investigation of  
114 landslide areas (McCann and Foster, 1990; Gallipoli et al., 2000; Hack 2000; Lapenna et al., 2003;  
115 Perrone et al., 2004; Lapenna et al., 2005; Lebourg et al., 2005; Perrone et al., 2006; Naudet et al.,  
116 2008; Chambers et al., 2011; Perrone et al., 2014), providing useful information on the geometrical  
117 characteristics of the investigated body and on potentially instable areas, due to the high water  
118 content.

119 Resistivity measurements are made by injecting a controlled current into the ground through two  
120 steel electrodes and measuring the potential drop at other two electrodes. An apparent resistivity  
121 value ( $\rho_a$ ) is calculated taking into account the intensity of the injected current (I), the potential drop  
122 (V) and a geometric coefficient (k) related to the spatial electrode configuration,  $\rho_a = k \cdot V/I$ . Different  
123 electrode arrays, such as Wenner, Schlumberger, dipole-dipole, etc., can be used for ERT surveys.  
124 To obtain a subsurface image of the electrical resistivity, the apparent electrical resistivity data have  
125 to be inverted in true electrical resistivity values by means of specific inversion software.

126 In this work, apparent electrical resistivity data were acquired through a multi-electrode system (48  
127 electrodes) using a Syscal Junior (Iris Instruments) resistivity meter connected to a multicore cable.  
128 A constant spacing (a) of 5 m between adjacent electrodes was used and a Wenner-Schlumberger  
129 (WS) array was adopted with different combinations of dipole length (1a, 2a and 3a) and number of  
130 depth levels “n” ( $n \leq 6$ ). The investigation depths were about 40 m. Data noise was assessed by  
131 means of repeatability tests (Robert et al., 2011). Five to ten stacked measurements were carried out



132 for each point and the respective relative standard deviation (Dev parameter) was estimated. The  
133 resistivity values characterized by a Dev parameter greater than 1% and all of the obvious outliers  
134 were removed. The apparent electrical resistivity data were inverted using the RES2DINV software  
135 (Loke, 2001) to obtain the 2D electrical resistivity images of the subsurface. The inversion routine  
136 is based on the smoothness-constrained least-squares inversion method implemented by using a  
137 quasi-Newton optimisation technique (Sasaki, 1992; Loke and Barker, 1996). The optimisation  
138 method adjusts the 2D electrical resistivity model trying to iteratively reduce the difference between  
139 the calculated and measured apparent resistivity values. The root-mean-squared (RMS) error  
140 provides a measurement of this difference.

141 All the ERT profiles, each with a length of 235 m, were placed perpendicularly to the main axis of  
142 the channel area of the landslide (Fig. 2). In particular, in the first field survey, on July 2011, three  
143 ERT were carried out in the upper-zone of the channel area between 700 m and 620 m a.s.l. The  
144 main aim of this survey was to check the functionality of a drainage trench located in the area and  
145 to obtain preliminary information on the geoelectrical characteristics of the material involved in the  
146 movement.

147 More than one year later, on October 2012, eleven ERT were realized in the central part of channel  
148 area, along parallel profiles spaced 50-60 m apart (Fig. 2). The aim of this survey was to  
149 characterize the geometry of this portion of the landslide, to improve the knowledge about the  
150 geological setting and to indirectly test the effectiveness of the specifically installed drainage  
151 system. This latter represented a very important information for the technicians of DPC, because  
152 this portion of landslide, despite the drainage interventions carried out, is characterized by a trend of  
153 continuous movement (Lollino et al., 2013; Lollino et al., 2014).

154

#### 155 **4. Results**

156 Here the results obtained during the two surveys carried out on July 2011 and October 2012 are  
157 discussed.

158 For all the ERT, the range of the electrical resistivity values is quite limited, varying between 3 and  
159 more than 34  $\Omega$ m. Generally, since the electrical resistivity of a rock is controlled by different  
160 factors (water content, porosity, clay content, etc.), there are wide ranges in electrical resistivity for  
161 any particular rock type and, accordingly, electrical resistivity values cannot be directly interpreted  
162 in terms of lithology. For these reasons, we used data from literature (Giocoli et al., 2008;  
163 Mucciarelli et al., 2009), geological surveys and exploratory boreholes to calibrate the ERT and to  
164 directly correlate electrical resistivity values with the lithostratigraphic characteristics. Thus, the  
165 following electrical resistivity ranges were assigned:  $\rho > 12 \Omega$ m to the FFa1,  $\rho < 6 \Omega$ m to FFa2,  $\rho$



166 > 20  $\Omega\text{m}$  to FVb and  $\rho < 8 \Omega\text{m}$  to FVc . In particular, the active landslide material is characterized  
167 by electrical resistivity values ranging between 6 and 12  $\Omega\text{m}$ , whereas the inactive earth-flow toe  
168 and of the old earth-flow show  $\rho > 8 \Omega\text{m}$  and  $\rho < 12 \Omega\text{m}$ , respectively.

169

170 *July 2011: first survey*

171 Figure 2 shows the profiles (blue lines) along that ERT were carried out during the first  
172 measurement campaign on July 2011. The profiles cross (active and inactive) landslide material and  
173 terrains belonging to the FF and FV. The lithological composition of these formations contributes to  
174 justify the low resistivity range characterizing the ERT.

175 Despite low resistivity contrasts, the three ERT allowed us to define the geometry of active and  
176 inactive landslide bodies, to identify sub-vertical discontinuities, often corresponding with the  
177 lateral limits of the earth-flow, and to locate areas characterized by higher water content (Fig. 3).

178

179

**Figure 3** - Resistivity models of the three ERT carried out across the Montaguto landslide in July 2011.

180

181

182 In particular, ERT 1 was placed parallel to one of the first drainage trenches, installed in the  
183 investigated area at a quote of about 700 m a.s.l., and shows both vertical and horizontal resistivity  
184 variations. In detail, between 85 and 180 m a relatively resistive superficial sector ( $8 < \rho < 25 \Omega\text{m}$ ),  
185 about 10-12 m thick, likely due to the drainage trench and active landslide material, is clearly  
186 identifiable. At the bottom, a relatively conductive layer ( $\rho < 6 \Omega\text{m}$ ), laterally limited by more  
187 resistive zones ( $\rho > 12 \Omega\text{m}$ ), could be associated with the clayey lithofacies (FFa2). By comparing  
188 the ERT with geological information, the more resistive zone located in SE portion could be related  
189 to the calcareous-marly lithofacies (FFa1) and the sub-vertical resistivity discontinuity could be due  
190 to the presence of a NE-SW normal fault, as reported in the map of figure 2, according to Guerriero  
191 et al. (2014). In the NW part of the ERT, the deep more resistive zone can be associated with FFa1.  
192 Finally, the shallow lenticular low resistivity zone in the NW sector can be interpreted as FFa2.

193 ERT 2 was carried out between 625-650 m a.s.l. It is characterized by two shallow areas of  
194 conductive material ( $\rho < 12 \Omega\text{m}$ ) with lenticular shape, overlying a relatively resistive material ( $\rho >$   
195  $12 \Omega\text{m}$ ). The first one, in the WSW sector of the ERT up to 100 m from the origin of the profile,  
196 may be associated with the inactive landslide body (IT in Fig. 2). The second one, in the central  
197 portion of the ERT between 105 m and 170 m from the origin and with a maximum thickness of 10  
198 m, is related to the active landslide. The more resistive material, in the deep part of ERT, is



199 associated with FFa1. Finally, the conductive area located at the eastern part of the ERT and  
200 bounded by the NE-SW normal fault can be associated with FFa2.

201 ERT 3 was realized between 613 – 628 m a.s.l. and is characterized by a chaotic resistivity  
202 distribution with weak lateral discontinuities. Between 85 m and 210 m from the origin of the  
203 profile, a shallow (max 8 m thick) relative resistive material is associated with the active earth-flow  
204 underlying a more conductive material, probably related to an old inactive landslide body. In the  
205 WSW sector, the shallow moderately resistive material ( $\rho > 8 \Omega\text{m}$ ), with a maximum thickness of  
206 about 12 m, is associated with the inactive earth-flow toe (IT) (Guerriero et al., 2014). The medium  
207 resistive material, which characterizes the bottom and the ENE sector of the ERT, can be related to  
208 FFa1.

209

210 *October 2012: second survey*

211 During the second survey, eleven ERT were carried out, with direction transversal to the landslide  
212 body along profiles parallel to each other and spaced approximately 50-60 m, in the central part of  
213 the channel area (Fig. 2). Before the geophysical survey, several actions (excavation, surface  
214 drainage, etc) aimed at the stabilization of the landslide in this sector of slope were adopted  
215 However, despite the drainage interventions carried out, this sector is characterized by a trend of  
216 continuous movement (Lollino et al., 2013; Lollino et al., 2014).

217 All the electrical images are reported in figures 4 and 5 and show almost the same resistivity  
218 pattern: the central part is always characterized by conductive material of lenticular shape, confined  
219 within more resistive material by means of sub-vertical contacts. Only ERT 11 shows a different  
220 resistivity configuration, probably because performed entirely inside the landslide body.

221

222

223 **Figure 4** - Resistivity models of six ERT carried out in the central part of the channel area of the Montaguto landslide  
in October 2012.

224

225 **Figure 5** - Resistivity models of five ERT carried out in the central part of the channel area of the Montaguto landslide  
in October 2012

226

227 All the resistivity models well highlight the presence of drainage channels that show up as very  
228 shallow resistive nuclei. Shallow moderate resistive material ( $6 < \rho < 12 \Omega\text{m}$ ) between drainage  
229 channels visible in all the ERT, except for ERT 7, can be associated with drained active landslide  
230 material reaching a maximum depth of about 15 m, according to Guerriero et al. (2014) and Lollino  
231 et al. (2014). Conductive material ( $\rho < 6-7 \Omega\text{m}$ ), characterizing the central and deep part of the



ERT, can be associated with the presence of a higher water content than surrounding material. This assumption is also supported by the piezometric information coming from boreholes S8, S7 and S6 and piezometers P1 and P2 (Lollino et al., 2014). The lenticular shape of this material could be also related to an old inactive landslide body, below the currently active one, reaching a maximum thickness of about 30 m. This old landslide material seems to be confined in a paleo-channel characterized by relatively resistive boundaries. The more resistive material in the deep part of ERT could be related to FFa1 (ERT 1 to ERT 4) or to FVb (ERT 5 to ERT 9).

The NE part of almost all ERT is characterized by high electrical resistivity values that are associated with material not affected by the movement and belonging to FFa1 (ERT 1 to ERT 5) and to FVb (ERT 6 to ERT 10). Conductive material visible at the end of ERT 1 - ERT 4 profiles could be related to FFa2.

The sub-vertical resistivity discontinuities in the NE sector of all ERT (except for ERT 11) could be associated with the extension of the NE-SW normal fault, partially reported in figure 3 in Guerriero et al. (2014).

The SW portions of all ERT consist of low-medium resistive material related to the sandy with silty clay beds (FVc).

248

## 249 **5. Conclusions**

250 This paper reports the results of two geoelectrical surveys carried out on the Montaguto landslide, in  
251 order to give a contribution in the geometrical characterization of the landslide body and in the  
252 definition of the geological setting. In addition, the effectiveness of the drainage system was  
253 indirectly tested.

254 Although electrical resistivity contrasts in the ERT images are not very pronounced, it was possible  
255 to observe the presence of both lateral and vertical discontinuities, which can be ascribed to  
256 lithological boundaries and/or physical variations of the same material with varying water content.

257 Regarding the geometrical characterization of landslide body and the reconstruction of geological  
258 setting in the channel area, the resistivity distribution in ERT images has highlighted the following  
259 points:

260 - the current active landslide material, reaching a maximum thickness of 15 m, is characterized by  
261 low-medium resistivity values ( $6 < \rho < 12 \Omega\text{m}$ ) and seems to be visible in almost all ERT obtained  
262 in both the measurement campaigns;

263 - the old landslide body, characterized by very low resistivity values ( $\rho < 6 \Omega\text{m}$ ) and a well defined  
264 lenticular shape with a maximum thickness of about 25-30 m, is clearly visible in the ERT obtained  
265 in the second measurement campaign;



266 - the lateral resistivity discontinuities, especially characterizing the NE sector of the ERT obtained  
267 on October 2012, represent the lateral limits of the both active and old landslide body. In some  
268 cases, these lateral limits are sub-vertical and can be associated with the presence of tectonic  
269 structures (normal fault) according to the morphology of the slope and the previous geological  
270 studies carried out in the area. Conversely, in the SW portion the superficial lateral limits of the  
271 landslide body not seem to be marked by clear resistivity contrasts, due to the outcropping  
272 lithotypes and to the presence of a high water content.

273 - ERT allowed the identification of the all drainage channels built in the upper and middle sector of  
274 landslide body. These structures are located in the first very shallow layers of the subsoil and are  
275 characterized by relatively high resistivity values ( $\rho > 12 \Omega\text{m}$ ). Considering that the material  
276 included between the drainage channels is characterized by medium resistivity values ( $6 < \rho < 12$   
277  $\Omega\text{m}$ ) respect to the more conductive surrounding material, it is possible to assert that the  
278 interventions carried out on the slope are working well. So the more resistive shallow part is likely  
279 to be moving material, continuously drained and thus dryer.

280 Finally, considering all the information obtained by geophysical and geological surveys, also  
281 according to Guerriero et al. (2014), we can conclude that the lithotypes outcropping on the slope,  
282 mainly sands and clays, represent the predisposing factor for landsliding. The increase of water  
283 content in the subsoil, due to the occurrence of intense rainfall events, can be considered the  
284 triggering factor. Whereas, the tectonic structures highlighted in the area do not seem to play a role  
285 in landslide triggering but clearly influence the shaping of the slope and the evolution of the  
286 landslide body.

287 All the information from our results are very important for the technicians of DPC and can be used  
288 for the planning of actions directed to the stabilization of the slope.

289

290 **Acknowledgements**

291  
292



293 **References**

- 294 Amore, O., Bassi, C., Ciampo, G., Ciarcia, S., Di Donato, V., Di Nocera, S., Esposito, P., Matano,  
295 F., Staiti, D., Torre, M., 1998. Nuovi dati stratigrafici sul Pliocene affiorante tra il fiume Ufita ed il  
296 torrente Cervaro (Irpinia, Appennino meridionale). *Boll. Soc. Geol. Ital.* 117, 455-466 (in Italian).
- 297 Chambers, J.E., Wilkinson, P.B., Kuras, O., Ford, J.R., Gunn, D.A., Meldrum, P.I., Pennington,  
298 C.V.L., Weller, A.L., Hobbs, P.R.N., Ogilvy, R.D., 2011. Three-dimensional geophysical anatomy  
299 of an active landslide in Lias Group mudrocks, Cleveland Basin, UK. *Geomorphology* 125, 472-  
300 484.
- 301 Crostella, A., Vezzani, L., 1964. La geologia dell'Appennino Foggiano. *Boll. Soc. Geol. Ital.* 83,  
302 121-141 (in Italian).
- 303 Dazzaro, L., Di Nocera, S., Pescatore, T., Rapisardi, L., Romeo, M., Russo, B., Senatore, M.R.,  
304 Torre, M., 1988. "Geologia del margine della Catena Appenninica tra il F. Fortore ed il T. Calaggio  
305 (Monti della Daunia – Appennino Meridionale). *Mem. Soc. Geol. Ital.* 41, 411-422 (in Italian).
- 306 Di Nocera, S., Torre, M., 1987. Geologia dell'area compresa tra Deliceto e Scampitella (Appennino  
307 Foggiano). *Boll. Soc. Geol. It.*, 106, 351-364 (in Italian).
- 308 Di Nocera, S., Matano, F., Pescatore, T., Pinto, F., Torre, M., 2011. Caratteri geologici del settore  
309 esterno dell'Appennino campano-lucano nei Fogli CARG. *Rend. Online Soc. Geol. Ital.* 12, 39-43  
310 (in Italian).
- 311 Gallipoli, M.R., Lapenna, V., Lorenzo, P., Mucciarelli, M., Perrone, A., Piscitelli, S., Sdao, F.,  
312 2000. Comparison of geological and geophysical prospecting techniques in the study of a landslide  
313 in southern Italy. *Eur. J. Environ. Eng. Geophysics* 4, 117-128.
- 314 Giocoli, A., Magrì, C., Piscitelli, S., Rizzo, E., Siniscalchi, A., Burrato, P., Vannoli, P., Bassi, C.,  
315 and Di Nocera, S., 2008. Electrical Resistivity Tomography Investigations in the Ufita Valley  
316 (Southern Italy). *Ann. Geophys.-Italy*, 51, 213-223.
- 317 Giordan, D., Allasia, P., Manconi, A., Baldo, M., Santangelo, M., Cardinali, M., Corazza, A.,  
318 Albanese, V., Lollino, G., Guzzetti, F., 2013. Morphological and kinematic evolution of a large  
319 earthflow: The Montaguto landslide, southern Italy. *Geomorphology* 187, 61-79,  
320 DOI:10.1016/j.geomorph.2012.12.035.
- 321 Guerriero, L., Revellino, P., Coe, J.A., Focareta, M., Grelle, G., Albanese, V., Corazza, A.,  
322 Guadagno, F.M., 2013. Multi-temporal Maps of the Montaguto Earth Flow in Southern Italy from  
323 1954 to 2010. *J. Maps* 9 (1), 135-145, DOI: 10.1080/17445647.2013.765812.
- 324 Guerriero, L., Coe, J.A., Revellino, P., Grelle, G., Pinto, F., Guadagno, F.M., 2014. Influence of  
325 slip-surface geometry on earth-flow deformation, Montaguto earth flow, southern Italy.  
326 *Geomorphology*, 219, 285-305, DOI:10.1016/j.geomorph.2014.04.039.
- 327 Hack, R., 2000. Geophysics for slope stability. *Surveys in Geophysics* 21, 423–448.
- 328 Lapenna, V., Lorenzo, P., Perrone, A., Piscitelli, S., Rizzo, E., Sdao, F., 2003. High-resolution  
329 geoelectrical tomographies in the study of the Giarrossa landslide (Potenza, Basilicata). *Bull. Eng.*  
330 *Geol. Environ.* 62, 259-268.
- 331 Lapenna, V., Lorenzo, P., Perrone, A., Piscitelli, S., Rizzo, E., Sdao, F., 2005. 2D electrical  
332 resistivity imaging of some complex landslides in Lucanian Apennine chain, southern Italy.  
333 *Geophysics* 70 (3), B11–B18.
- 334 Lebourg, T., Binet, S., Tric, E., Jomard, H., El Bedoui, S., 2005. Geophysical survey to estimate the  
335 3D sliding surface and the 4D evolution of the water pressure on part of a deep-seated landslide.  
336 *Terra Nova* 17, 399–406.

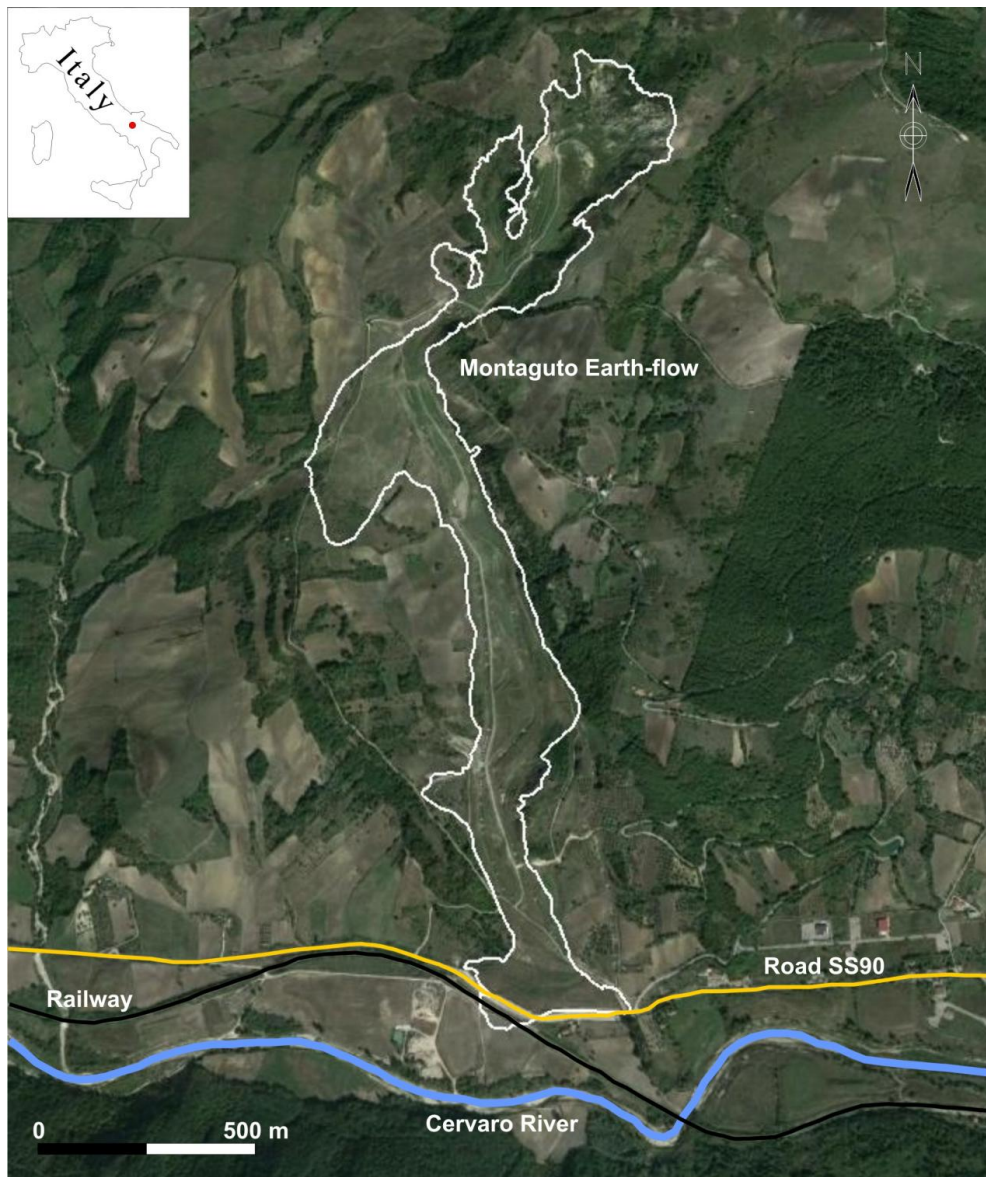


- 337 Lollino, G., Allasia, P., Giordan, D., Guzzetti, F., Lollino, P., Baldo, M., 2013. Studio della frana di  
338 Montaguto (AV) con tecniche di monitoraggio integrato. BURC N.1 07/01/2014, Allegato Tecnico,  
339 1-14, <http://burc.regionecampania.it/eBurcWeb/publicContent/archivio/archivioiface> (in Italian).
- 340 Lollino, P., Giordan, D., Allasia, P., 2014. The Montaguto earthflow: A back-analysis of the  
341 process of landslide propagation. Eng. Geol. 170, 66-79, doi:10.1016/j.enggeo.2013.12.011.
- 342 Loke, M.H., 2001. Tutorial: 2-D and 3-D electrical imaging surveys, available at:  
343 <http://www.geoelectrical.com> (last access: June2013).
- 344 Loke, M.H., Barker, R.D., 1996. Rapid least-squares inversion of apparent resistivity  
345 pseudosections by a quasi-newton method, Geophys. Prospect., 44, 131-152.
- 346 McCann, D.M., Forster, A., 1990. Reconnaissance geophysical methods in landslide investigations.  
347 Eng. Geol. 29, 59-78.
- 348 Mucciarelli, M., Böhm, G., Caputo, R., Giocoli, A., Gueguen, E., Klin, P., Marello, L., Palmieri, F.,  
349 Piscitelli, S., Priolo, E., Romano, G., Rizzo E., 2009. Caratteri geologici e geofisici dell'area di San  
350 Giuliano di Puglia. Riv. Ital. Geotecnica, 3, 32-42.
- 351 Naudet, V., Lazzari, M., Perrone, A., Loperte, A., Piscitelli, S., Lapenna, V., 2008. Integrated  
352 geophysical and geomorphological approach to investigate the snowmelt-triggered landslide of  
353 Bosco Piccolo village (Basilicata, southern Italy). Eng. Geol. 98, 156-167.
- 354 Perrone, A., Iannuzzi, A., Lapenna, V., Lorenzo, P., Piscitelli, S., Rizzo, E., Sdao, F., 2004. High-  
355 resolution electrical imaging of the Varco d'Izzo earthflow (southern Italy). J. Appl. Geophysics 56,  
356 17-29.
- 357 Perrone, A., Zeni, G., Piscitelli, S., Pepe, A., Loperte, A., Lapenna, V., Lanari, R., 2006. Joint  
358 analysis of SAR interferometry and electrical resistivity tomography surveys for investigating  
359 ground deformation: the case-study of Satriano di Lucania (Potenza, Italy). Eng. Geol. 88, 260-273.
- 360 Perrone, A., Lapenna, V., Piscitelli, S., 2014. Electrical resistivity tomography technique for  
361 landslide investigation: A review. Earth-Science Reviews 135, 65-82,  
<http://dx.doi.org/10.1016/j.earscirev.2014.04.002>.
- 363 Pescatore, T., Russo, B., Senatore, M.R., Ciampo, G., Esposito, P., Pinto, F., Staiti, D., 1996. La  
364 successione messiniana della valle del Torrente Cervaro (Appennino Dauno, Italia Meridionale).  
365 Boll. Soc. Geol. Ital. 115, 369-378 (in Italian).
- 366 Robert, T., Dassargues, A., Brouyère, S., Kaufmann, O., Hallet, V., Nguyen, F., 2011. Assessing  
367 the contribution of electrical resistivity tomography (ERT) and self-potential (SP) methods for a  
368 water well drilling program in fractured/karstified limestones. J. Appl. Geophysics, 75(1), 42-53.  
369 <http://doi.org/10.1016/j.jappgeo.2011.06.008>.
- 370 Santo, A., Senatore, M.R., 1988. La successione stratigrafica dell'Unità Dauna a Monte Sidone  
371 (Castelluccio Valmaggiore - Foggia). Mem. Soc. Geol. It., 41 431-438 (in Italian).
- 372 Sasaki, Y., 1992. Resolution of resistivity tomography inferred from numerical simulation,  
373 Geophys. Prospect., 40, 453-463.
- 374 Ventura, G., Vilardo, G., Terranova, C., Bellucci Sessa, E., 2011. Tracking and evolution of  
375 complex active landslides by multi-temporal airborne LiDAR data: The Montaguto landslide  
376 (Southern Italy). Remote Sens. Environ., 115:12, 3237-3248.
- 377



378 **Figure 1**

379



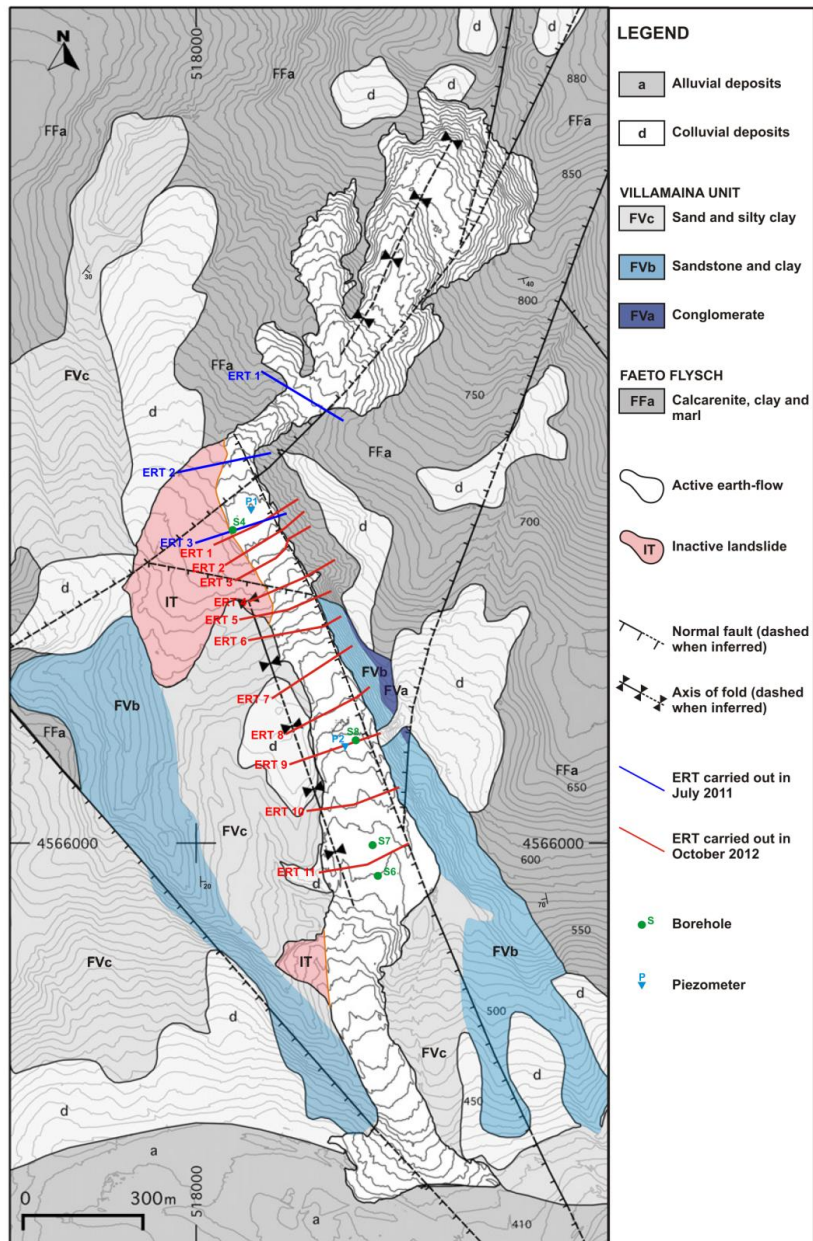
380

381



382 **Figure 2**

383



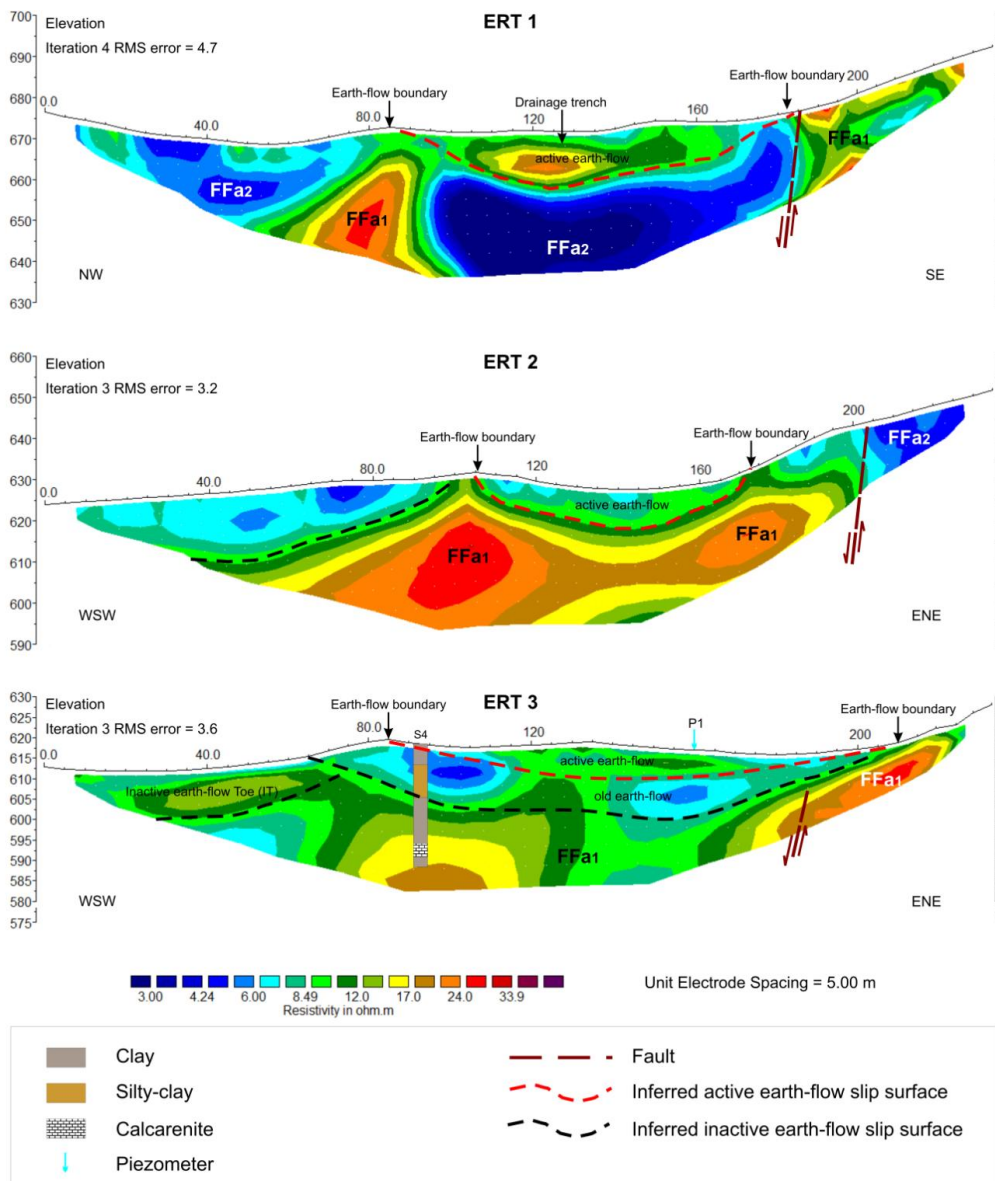
384

385



386 **Figure 3**

387

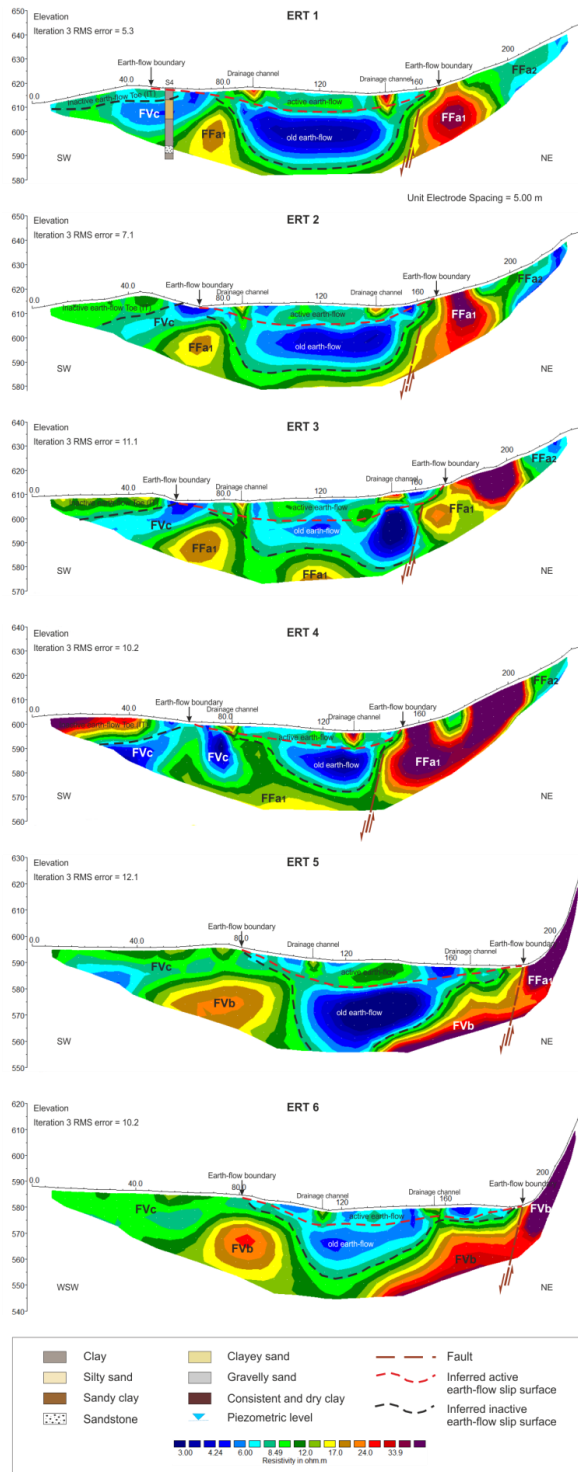


388

389



390 **Figure 4**

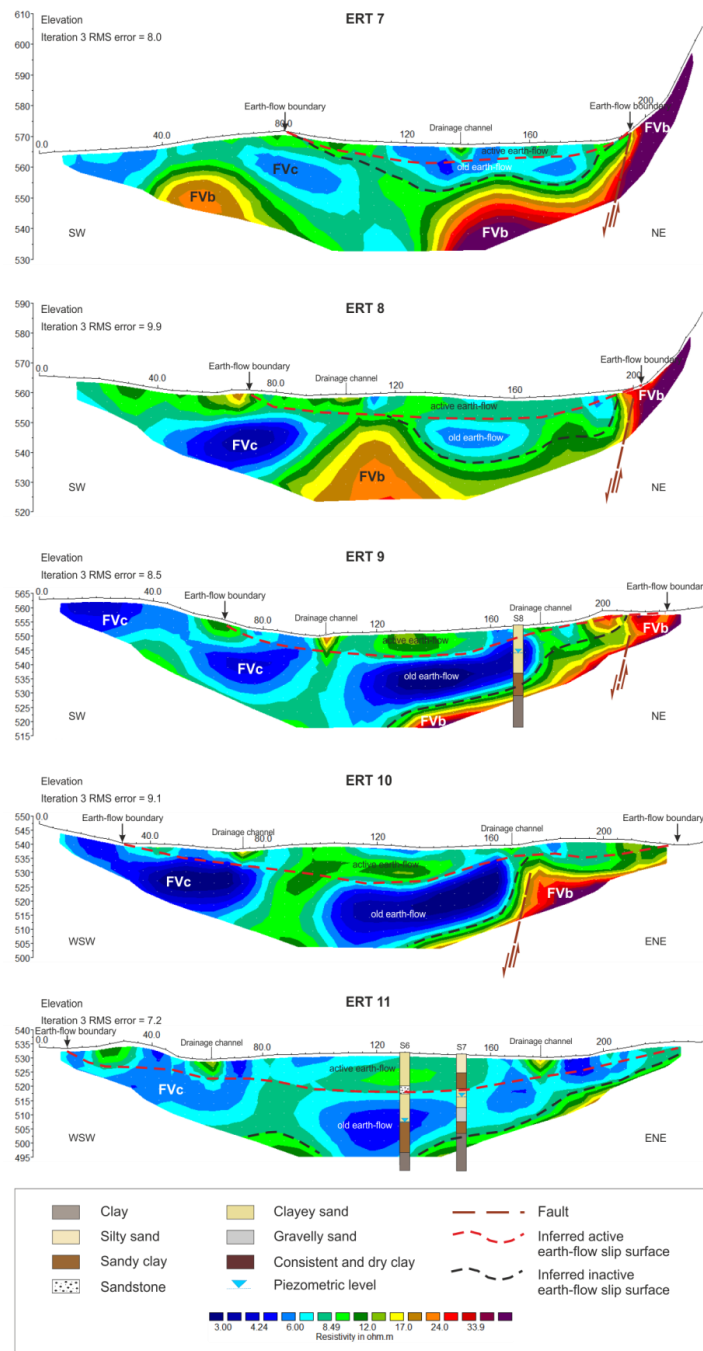




392

**Figure 5**

393



394